TÜBİTAK

Turkish Journal of Chemistry

http://journals.tubitak.gov.tr/chem/

Research Article

Turk J Chem
(2018) 42: 547 – 561
© TÜBİTAK
doi:10.3906/kim-1709-43

Adsorptive properties of mesoporous silica modified with Lewis base molecule and its application in the preconcentration of Cu(II), Co(II), and Cd(II) from aqueous media

Janaíne do Rócio IVASSECHEN[1,2], Alexandre de Oliveira JORGETTO[1,2], Marcos Henrique Pereira WONDRACEK[1,3], Adrielli Cristina Peres da SILVA[2], Luiz Fabrício ZARA[4], Valber de Albuquerque PEDROSA[2], Bruno Prior ROCHA[1], Margarida Juri SAEKI[2], Gustavo Rocha CASTRO[1,2,*]

[1]Institute of Chemistry, Sao Paulo State University (UNESP), Araraquara, Sao Paulo, Brazil
[2]Department of Chemistry and Biochemistry, Institute of Biosciences of Botucatu, Sao Paulo State University (UNESP), Botucatu, Sao Paulo, Brazil
[3]Faculty of Exact Sciences and Technology, Federal University of Grande Dourados (UFGD), Dourados, Mato Grosso do Sul, Brazil
[4]Faculty of Planaltina, University of Brasília, Planaltina, Goias, Brazil

Received: 22.09.2017 • **Accepted/Published Online:** 08.01.2018 • **Final Version:** 27.04.2018

Abstract: Cocondensation and postfunctionalization methods were employed to synthesize a mesoporous silica with large surface area (795.1 ± 1.1 m^2 g^{-1}) modified with 4-amino-5-hydrazino-1,2,4-triazole-3-thiol, which was successfully applied to adsorb and preconcentrate Cu(II), Co(II), and Cd(II) from aqueous media. Infrared spectroscopy of the adsorbent material demonstrated N-H stretching bonds related to primary amines existing in the ligand molecule, elemental analysis revealed the presence of 0.132 mmol g^{-1} of nitrogen, scanning electron microscopy indicated globularly shaped particles with average size of 10 μm, and the point of zero charge was found to be 7.2. Kinetic data were applied to the pseudo-second-order model, indicating that a chemisorption mechanism is probably involved in the uptake of metal ions from aqueous solutions. According to the Langmuir model, the adsorption capacities for the different ions obey the following order: Cu(II) > Co(II) > Cd(II). Through a preconcentration system, a preconcentration factor of 18-, 15-, and 20-fold was attained for Cu(II), Cd(II), and Co(II), respectively. The proposed method was applied in the determination of trace metals in natural river water (Tietê River) and the results were validated through standard reference material analysis. The results also indicated that the packed column proved to be stable over 24 adsorption/desorption cycles, demonstrating that the developed material is potentially suitable for the determination of trace-level metal ions in aqueous samples.

Key words: Cocondensation method, modified surface, metal adsorption, preconcentration

1. Introduction

Several types of substances are released daily in the environment through effluents in gaseous, liquid, or solid state. From an environmental perspective, pollution is drastically aggravated by population growth, accompanied by an increase in the demand for durable/nondurable goods and leading to the massive production of all sorts of consumables, which generally does not occur in accordance with sustainable principles.

*Correspondence: castrogr@ibb.unesp.br

It is obvious that the emission of several such types of substances can be harmful to the environment and some of them stand out due to their high toxicity; among them, we can cite here heavy metals such as Cu(II), Cd(II), Pb(II), and Ni(II). Dissolved heavy metal ions can be found naturally in the environment, mainly due to the occurrence of rock weathering, but anthropogenic activities have also been drastically increasing the presence of such species in the environment by emissions associated with nonsustainable industrial, agricultural, and domestic processes.

In general, human beings are contaminated by heavy metals mainly through the ingestion of contaminated food and water as soils, water, and sediments are the final destination for most kinds of emitted pollutants. Heavy metals in environmental matrices such as soils and water have been investigated for decades as they are nondegradable and may be involved in bioaccumulation and biomagnification processes causing serious deleterious effects for living organisms.[1−4] Harmful effects such as high blood pressure and kidney and nervous system impairments have been attributed to metal ions such as cadmium, copper, lead, and others, which are considered toxic to aquatic biota.[5] In response to this concern, several research groups have focused on the development of methods to efficiently remove metal species from water. Among these, methods based on coprecipitation reactions, liquid–liquid microextraction,[6,7] cloud-point extraction, electrolytic deposition,[8] and solid-phase extraction[9−12] have been applied for the extraction/preconcentration of metal species.[13−15]

With regard to solid-phase extraction, many different types of solid phases have been employed in separation and preconcentration processes, such as natural materials (cassava husks, grass, agricultural waste),[16−18] activated carbon produced through biomass carbonization,[19,20] modified cellulose, and silica.[9,21−27] In this regard, silica has been widely applied for solid-phase extraction procedures because of some of its outstanding properties such as thermal stability, no swelling, large specific surface area, and the presence of surficial reactive hydroxyl groups on its surface, which enables chemical modification. Nevertheless, despite the improvements in material synthesis to turn silica into a good adsorbent, metal ion adsorption does not occur satisfactorily on its bare form, and generally a modification step is required to enhance its adsorption properties, which is usually done by the attachment of a ligand molecule containing Lewis basic centers.

Several types of chelating molecules have already been anchored to the surface of silica and many strategies have already been approached to increment solid-phase extraction by silica-based adsorbents in the last two decades, which include the preparation of materials through one-step synthesis by cocondensation method,[20] production of silica-coated magnetic nanoparticles,[20,28−30] and development of mesoporous modified silica.[31,32] As can be noted from the persistent pursuit to develop adequate methods and materials for water treatment and wastewater remediation, it is clear that such topics are of great concern and importance for society and the environment.

These materials allowing the solid-phase extraction procedure have been applied as an important tool to ensure the safe quantification of trace metals using flame atomic absorption spectrometry (FAAS) and other related techniques with low sensitivity compared with graphite furnace atomic absorption spectrometry (GFAAS) and inductively coupled plasma mass spectrometry (ICPMS).[33−36]

In view of this, the aim of the present study was to develop a mesoporous silica modified with the chelating molecule 4-amino-5-hydrazino-1,2,4-triazole-3-thiol to be applied in the extraction and preconcentration of toxic (cadmium) and potentially toxic (copper and cobalt) metal species from aqueous solutions. The material was synthesized through a cocondensation step of tetraethylorthosilicate and 3-chloropropyltrimethoxysilane, which was followed by postfunctionalization with the ligand molecule. The material was characterized by Fourier transform infrared (FTIR) spectroscopy, scanning electron microscopy (SEM), and elemental analysis

to determine the morphology and constitution of the material's particles. To better comprehend the adsorptive interfacial processes, a point of zero charge (PZC) experiment was also carried out, and then the material was tested through batch and in-flow experiments to reveal its adsorption properties as well as its potential for preconcentration and application in the determination of metal ions at trace levels in real samples from the Tietê River.

2. Results and discussion

2.1. Material characterization

The silica synthesized through cocondensation (*Si*) was first subjected to surface area measurements through the BET method in order to determine its properties such as pore distribution and specific surface area. Before surface area measurements the material was calcined at 600 °C for 5 h to remove the organic phase derived from the silylating agent, which may block nitrogen molecules during analysis. The results obtained are depicted in Figure 1.

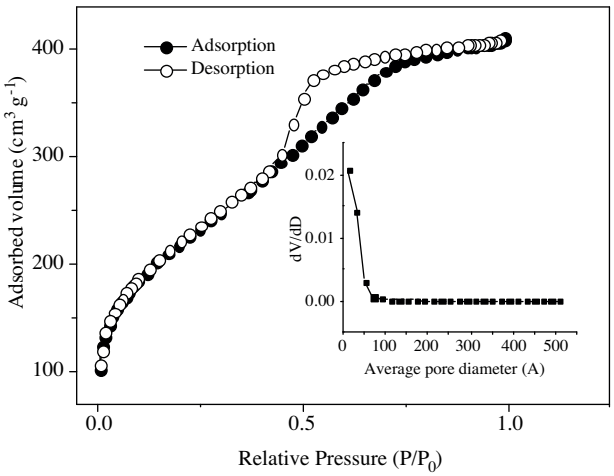

Figure 1. Nitrogen adsorption isotherm and pore size distribution for the silanized mesoporous silica.

According to the results, the surface area measurements demonstrated that the material presented a large specific surface area of 795.51 ± 1.14 m^2 g^{-1} and a type IV adsorption isotherm, which presents two inflection points. Analyzing the isotherm from the increasing direction of the relative pressure, the region before the first inflection point is related to the adsorption of a few layers over the material's surface, while from this point on there is the formation of multilayer adsorption and the plateau formed at high relative pressure values is assigned to the complete filling of the pores. The adsorption isotherm hysteresis is type H2, which is due to capillary condensation inside pores.[37,38] This type of hysteresis is associated with the interconnectivity between the pores of the particles and the irregularity of their forms as well as the variation in the size.[39] The presence of hysteresis generally implies that the mechanism of nitrogen adsorption occurs through a different mechanism than that of the desorption. While the occupation of the interior volume of the pores of the material can occur homogeneously during adsorption, the inoccupation of the pores does not occur so homogeneously (which may be associated with the referred type of pore), therefore causing hysteresis between the adsorption and desorption branches of the isotherm.[40] With respect to the analysis of pore size (inset in Figure 1), it was possible to verify that the material presents a great population of its pores within the range of 1.1 to 7.1 nm, which is within the

as-defined mesoporous material's range (established from 2 to 50 nm). In addition, the high adsorption slope seen at very low relative pressures indicates the presence of micropores for this material.

The morphology of the synthesized silica was investigated through SEM and can be observed in Figure 2. According to Figure 2a, a powder is composed of isolated particles and some agglomerates. Particles have predominantly a globular shape, and through Figure 2b its average diameter was estimated to be about 10 μm. Materials with particle diameters above 5 μm are desired for solid-phase extraction with fixed beds (column mode) as they enable the use of relatively high flows without presenting significant problems related to the clogging of the column. Furthermore, it is also possible to see the presence of agglomerates of particles.

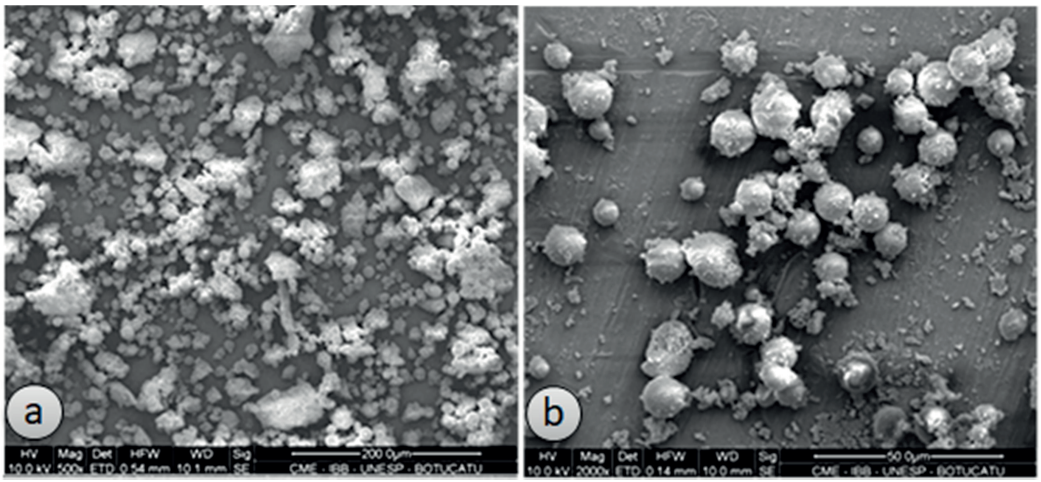

Figure 2. SEM images of the modified mesoporous silica.

Regarding the material's chemical composition, the ligand 4-amino-5-hydrazino-1,2,4-triazole-3-thiol (AHTT) was chosen due to its potential as a complexing agent, which is evidenced by its nitrogenated and sulfurated groups. After its attachment onto the silica's surface, the modified material was subjected to elemental analysis and the results indicated the presence of 0.132 mmol g^{-1} of nitrogenated groups. Based on this value, the amount of ligand molecules attached to the silica's surface was calculated as 0.022 mmol per gram of silica modified with the ligand (Si-AHTT).

The silica silanized with 3-choloropropyltriethoxysilane (Si-CPTS) and Si-AHTT also had its infrared spectra collected (Figure 3), which are shown along with the spectrum of the ligand for comparison. Such spectra suggest the incorporation of the ligand molecule to the silica's surface. The main changes observed are highlighted in Figure 3 and were assigned as follows: in the Si-CPTS's spectrum there is an absorption band located at 642 cm^{-1}, which is attributed to the C-Cl stretching vibration from the silylant agent (CPTS).

After surface functionalization, this band disappeared as a result of the attachment of the ligand, which occurred through a nucleophilic substitution of Cl atoms; by comparing the spectra of Si-CPTS and of Si-AHTT in the region around 1630 cm^{-1}, an O-H band for Si-CPTS is verified, whereas two sharper bands are observed for Si-AHTT (1637 and 1687 cm^{-1}), associated with NH_2 stretching vibrations. As can be seen from the spectrum of the AHTT ligand, these bands of the Si-AHTT material present a good correlation with those two in the same region for the ligand's spectrum (1600 and 1640 cm^{-1}), and probably the one observed at 1637 cm^{-1} for Si-AHTT overlaps with that of the O-H band for the Si-CPTS material, thus increasing its intensity. The fact that they are displaced to higher frequency values may be due to the dispersion of the ligand

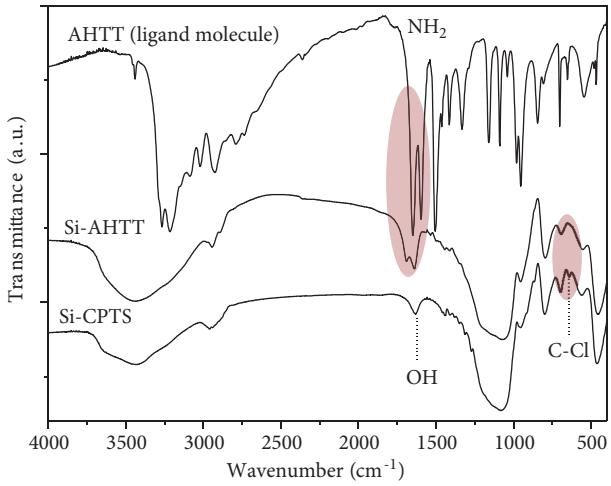

Figure 3. Infrared spectra of 4-amino-5-hydrazino-1,2,4-triazole-3-thiol molecule (AHTT), along with the spectra of the modified silica (Si-AHTT) and the silanized silica obtained through cocondensation method (Si-CPTS).

molecules on the large surface of the modified silica; this may set the immobilized ligand molecules apart from each other and therefore vibrational hindrances arising from intermolecular interactions may not be playing a significant role in this case. In other words, the dispersion of the molecules on the silica's surface makes the ligand's molecular structure freer to vibrate at higher frequencies, and that is why we observed the shift in the NH_2 band positions. Another observation regarding the FTIR analysis is that, besides the amine bands, no other band of the ligand molecules could be observed for the functionalized material, probably because most of them are found in the corresponding same spectral regions in which either typical silica bands or OH bands are quite intense, and therefore such bands effectively supersede those of the ligand, not allowing their detection and assignment.

Prior to its application in adsorption/extraction experiments, an investigation was carried out to uncover the material's global surface charge as a function of medium pH, as well as the pH at which the global charge is null (or the pH_{PZC}). This investigation is very important to better understand the adsorption process, since in most of cases it can be directly related to it. From the results of this study we can then make assumptions about the pH values at which adsorption will be favored or compromised. From the collected data of the PZC experiment we could plot the graph of Figure 4, and the pH_{PZC} was determined as the pH at which the experimental curve intersects the straight line defined by $pH_{final} = pH_{initial}$.

As can be seen, pH_{PZC} was found to be 7.2 (where the line $pH_{initial}$ crosses the line pH_{final}). Nevertheless, the region between 5 and 9 of pH_{final} is constant and this implies that when the material is dispersed in a medium whose pH is lower than 5.0, its surface will be predominantly found protonated, which will give it a positive overall charge. On the other hand, if the pH is greater than 9.0, the amount of deprotonated groups on the surface of the material will exceed the number of protonated groups, and the overall electrical charge will be negative. Taking this information into account with regard to the adsorption of metal cations, a positive surface charge will compromise the adsorption process. Based on this argument, the material's negatively charged surface found at pH >7.2 looks much more appealing for the adsorption of cations. Nevertheless, if the concentration of hydronium ions is too high, phenomena such as solvation of metal ions, hydrolysis, and precipitation of hydroxides may take place, which will also not favor cation adsorption. In view of that, the pH of metal solutions was adjusted in the range of 5 to 6 before adsorption experiments.

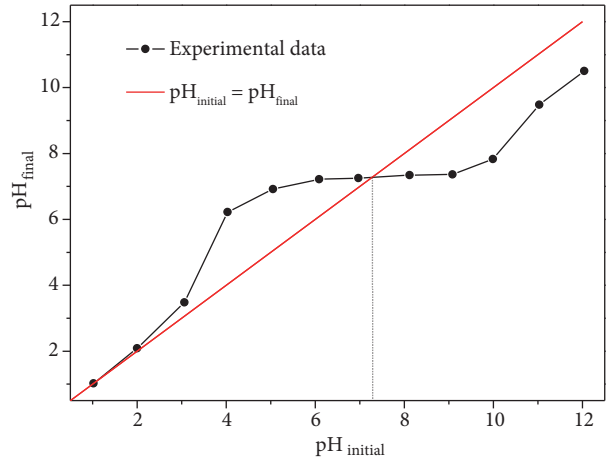

Figure 4. PZC experiment for Si-AHTT.

3. Adsorption experiments in batch mode

The quantity of adsorbed metal per mass unit of the adsorbent, N_f, was calculated according to Eq. (1):

$$\mathbf{N_f = \frac{n_i - n_s}{m}}, \tag{1}$$

where n_i represents the initial amount of metal ions in the solution (mmol), n_s is the amount of metal ions in the supernatant after equilibrium has been reached (mmol), and m is the mass of modified material (g). All experiments were performed at 26 °C.

An important aspect regarding the adsorption properties is the rate at which metal ions are adsorbed from the solution and the time required for the system to reach the equilibrium condition. As can be seen from the data of the kinetic experiment (Figure 5 and inset), equilibrium was attained at 20 min of dynamic contact for all metal species. The collected data were also inserted into the linearized pseudo-second-order kinetic model represented by Eq. (2), as follows:

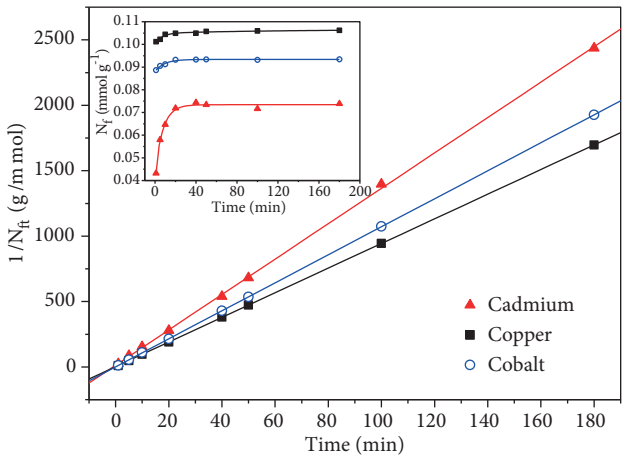

Figure 5. Kinetic isotherms for Cu(II), Cd(II), and Co(II) and their linearization according to the pseudo-second-order model.

$$\frac{t}{N_f} = \frac{1}{K_2 N_e^2} + \frac{1}{N_e} t, \tag{2}$$

where N_f represents the adsorption capacity, as calculated from Eq. (1), at a given time (mmol g^{-1}); N_e corresponds to the adsorption capacity at equilibrium (mmol g^{-1}); K_2 is the pseudo-second-order kinetic constant (g $mmol^{-1}$ min^{-1}); and t is the contact time condition used for each individual experiment (min).

As can be observed from Figure 5, excellent accordance was found between the experimental data and this model for all metals, which is also expressed by the determination coefficients obtained (R^2), i.e. 0.9998 for Cd(II) and 0.9999 for both Cu(II) and Co(II), while the respective values for K_2 were found to be 14.5, 39.6, and 89.1 g $mmol^{-1}$ min^{-1}. The calculated adsorption capacity at equilibrium, N_e, provided good accordance to the values observed from the isotherms, i.e. 0.074, 0.106, and 0.093 mmol g^{-1}. Besides indicating that the model mathematically describes the material's kinetic behavior very well under the studied conditions, this also means that implications associated with such a model can be assumed to hold for the studied systems. In this regard, it is expected that the main process responsible for the extraction of metal ions from solution is through chemisorption. According to the ligand's chemical structure, electron pairs available at nitrogen and sulfur adsorption sites are being shared with metal species, resulting in a covalent bond, as represented by the scheme in Figure 6.

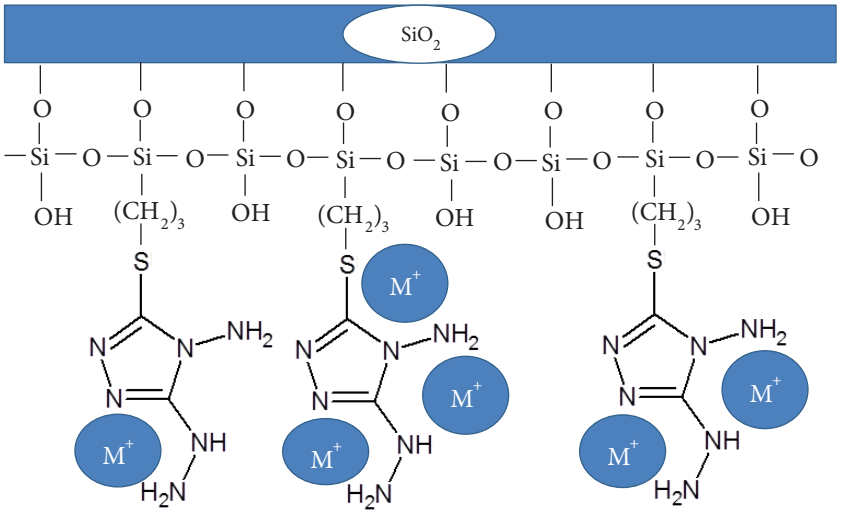

Figure 6. Scheme of the adsorptive interactions between the silica functionalized with AHTT and the metal ions in solution.

The adsorption capacities of Si-AHTT towards the studied species were determined by stirring the adsorbent with solutions of the metal ions at different concentrations for 40 min, when equilibrium was reached. The results obtained from this experiment are represented in Figure 7. According to the results, experimental maximum adsorption capacities ($N_{f(max)}$) for Cu(II), Co(II), and Cd(II) ions are 0.112, 0.117, and 0.077 mmol g^{-1}, respectively. Similarly to the kinetic experiment, the data from the adsorption capacity experiment were also analyzed in terms of a mathematical model, namely the linearized Langmuir model, which is expressed by Eq. (3) as follows:

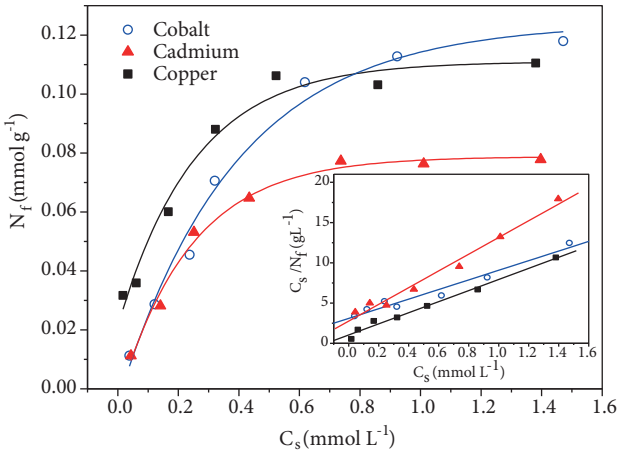

Figure 7. dsorption capacity isotherms for Cu(II), Cd(II), and Co(II) and their linearization according to the Langmuir model.

$$\frac{\mathbf{C_s}}{\mathbf{N_f}} = \frac{\mathbf{C_s}}{\mathbf{N_s}} + \frac{\mathbf{1}}{\mathbf{N_s b}} \frac{C_s}{N_f} = \frac{C_s}{N_s} + \frac{1}{N_s b}, \tag{3}$$

where C_s is the concentration of the supernatant at adsorption equilibrium (mmol L^{-1}), N_f is the amount of metal adsorbed calculated as from Eq. (1) for a given condition (mmol g^{-1}), N_s is the maximum amount of metal extracted from the solution (mmol g^{-1}), and b is the Langmuir constant, which is related to the affinity of the absorbent by the adsorbate.[41,42] By plotting the adsorption data as C_s/N_f vs. C_s, we could build the inset graph of Figure 7, from which we assessed the existence of linearity through the correlation coefficients and obtained values of 0.9972, 0.9725, and 0.9143 for Cu(II), Co(II), and Cd(II), respectively, which indicates a very good correlation between the data and the Langmuir model. Furthermore, the calculated maximum adsorption capacities (N_s) provided values with the same order of magnitude as those obtained experimentally, i.e. 0.145, 0.136, and 0.084 for Cu(II), Co(II), and Cd(II), respectively. Such a good fit between the experimental adsorption data and the Langmuir model is evidence that a monolayer of adsorbate is being formed on the material's surface, which also reinforces the chemisorption mechanisms previously indicated by the pseudo-second-order kinetic model. The trends observed for the adsorption capacities of the different metals may be explained by Pearson's concept, which predicts the behavior of soft/hard Lewis acids/bases.[43]

According to this concept, Cu(II) and Co(II) are classified as intermediary acids and interact preferably with intermediary bases through complexation reactions, whereas Cd(II) is classified as a soft acid and therefore has a greater affinity for soft bases. In view of that, it is reasonable to infer that the higher adsorption capacities of Cu(II) and Co(II) ions are probably related to their higher affinity for the ligand's amine groups (which consist of intermediary bases) as well as to the greater amount of N atoms in the ligand's structure in comparison to the amount of S atoms. Moreover, Cd(II) ions have a greater ionic radius than Cu(II) and Co(II), which can be associated with greater steric hindrances that compromise the diffusion and access to the sulfurated adsorption sites.

By comparing the maximum adsorption capacities of the different metal species (Table 1) to the amount of nitrogen found in the material through elemental analysis (0.132 mmol g^{-1}), we notice that there is a good correlation between such quantities, and this suggests that, besides the material's structure enabling good

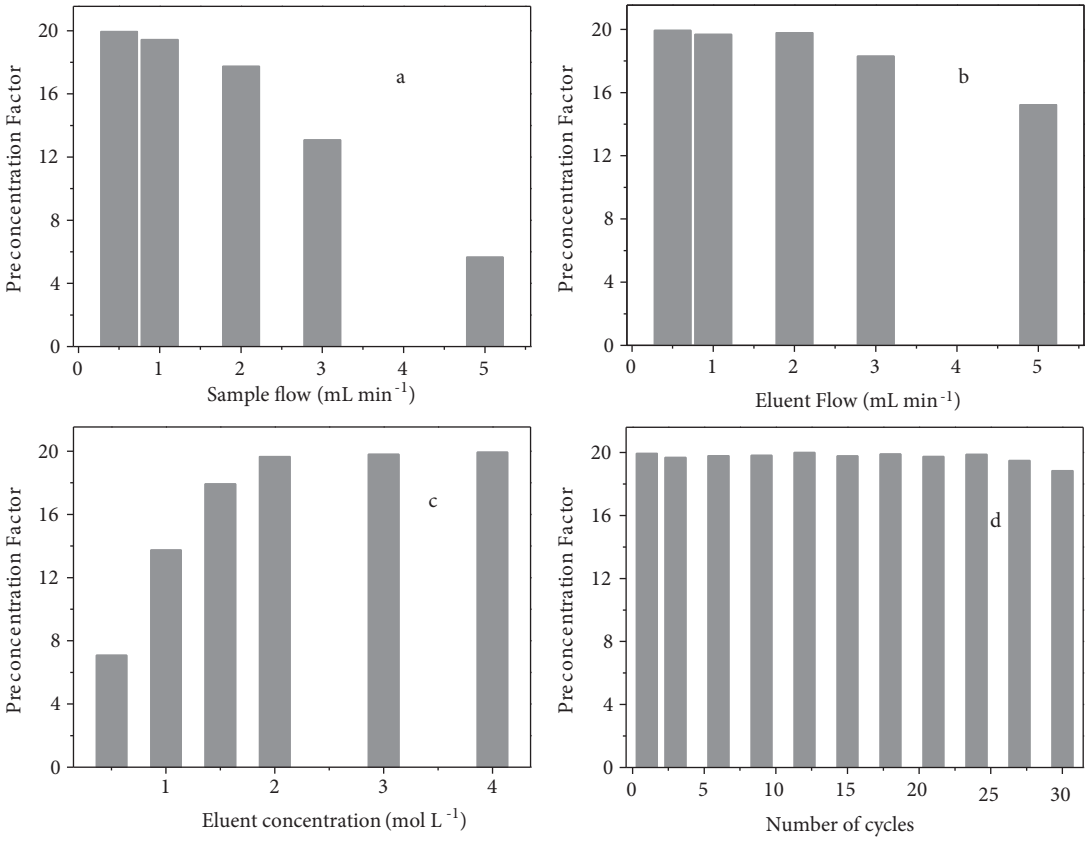

Figure 8. Optimization and reutilization experiments with Cu(II) solution (sample volume = 20 mL; sample concentration = 20 μg L^{-1}; eluent volume = 1.0 mL; eluent concentration = 2.0 mol L^{-1}). The parameters investigated were (a) the flow of the sample, (b) the flow of the eluent, (c) the concentration of the eluent, and (d) the maximum number of adsorption-desorption cycles without significant efficiency loss.

accessibility for nearly all of its adsorption sites, most of the nitrogenated groups of each single ligand are involved in the complexation of Cu(II) and Co(II) ions. On the other hand, Cd(II) adsorption is much higher than the amount of sulfur (0.022 mmol g^{-1}, as deduced from the 1:1 stoichiometric ratio between the ligand and its S atoms), which indicates that N atoms may also account for the complexation of the soft acid Cd(II) ions, despite the smaller affinity between soft acids and intermediary bases. Some possible interactions between the material's surface and metal species are depicted in Figure 6. Table 1 presents a comparison of the developed material with other adsorbents.

4. In-flow column experiments

Besides unveiling the adsorption properties of an adsorbent, studying its behavior under a column regime may be of great interest from the point of view of trace metal analysis. The importance of such investigation resides in the possibility of performing determination of trace concentrations by the preconcentration of toxic metals such as cadmium, mercury, and arsenic as well as that of potentially toxic metals such as copper, zinc, and cobalt among others, without resorting to high-cost techniques such as inductively coupled plasma-optical emission spectrometry (ICP-OES), ICPMS, or GFAAS. Thus, in order to assess the applicability of the Si-AHTT material

Table 1. Comparison of adsorption capacities for Cu(II), Co(II), and Cd(II) over different adsorbent materials.

	$N_{f\,(max)}$ (mmol g^{-1}) Si-AHMT*	$N_{f\,(max)}$ (mmol g^{-1})	Material	Reference
C (II)	0.112	0.0123	Silica (MS-AMP)	[40]
		0.3000	Phase Q mod. silica	[41]
		0.2801	Biomass mod. silica	[42]
Cd(II)	0.077	0.0006	Silica (MS-AMP)	[40]
		0.0670	Phase Q mod. silica	[41]
		0.1305	Biomass mod. silica	[42]
Co(II)	0.117	—-	——	——
		0.1200	Phase Q mod. silica	[41]
		—-	——	——

*Material under investigation.

for the quantification of trace metal concentration through a column regime, a study to determine the optimum preconcentration conditions was performed using Cu(II) solutions as a model analyte solution, and the collected data were used to create Figure 8. Metal solutions were percolated through the column at different flow rates, whereas sample volume, eluent flow, and eluent concentration were kept constant (20 mL, 0.5 mL min^{-1}, and 2.0 mol L^{-1} of HNO_3, respectively). The volume of the eluent was fixed at 1.0 mL for all experiments because smaller volumes would make metal determination via FAAS very difficult/impractical while greater volumes would cause an undesired reduction in the preconcentration factor (PF).

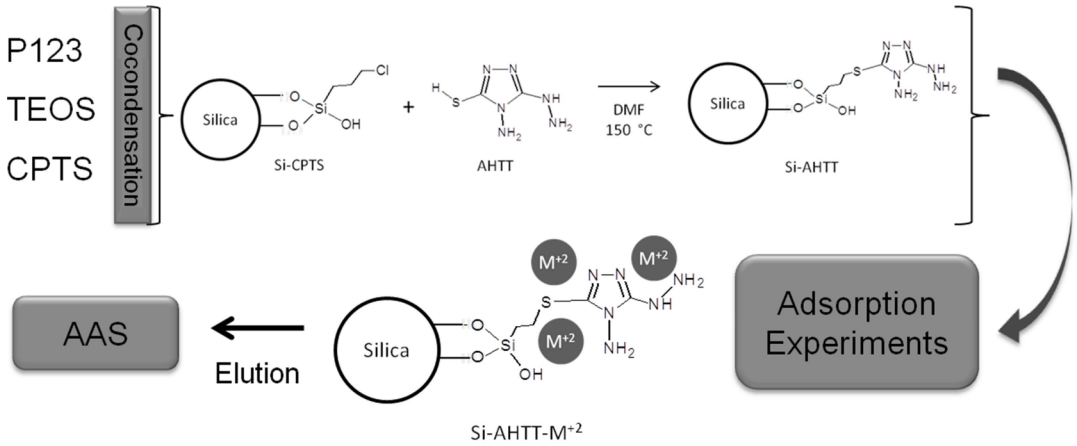

Figure 9. Reaction and application scheme for the synthesized material (SBA-type silica modified with 4-amino-5-hydrazino-1,2,4-triazole-3-thiol).

It is possible to observe from this experiment, as shown in Figure 8a, that increasing the sample flow rate a decrease in the PF value is verified, which can be attributed to the reduction in the interaction time between metal ions and the surface of the packed material. Although the flow of 1.0 mL min^{-1} provided a slightly smaller PF than that for 0.5 mL min^{-1}, this first flow value was chosen to proceed with the preconcentration

experiments once the difference between the PF values was very low ($<5\%$) and thus a higher throughput for the subsequent experiments was ensured. Eluent flow rate was investigated from 0.5 to 5.0 mL min^{-1} and, according to the results, represented in Figure 8b, up to a flow of 2.0 mL min^{-1} no reduction in the PF values was observed. For flow values greater than 2.0 mL min^{-1} the protonation process does not occur satisfactorily, probably because the contact time is reduced and H^+ ions do not interact with most of the adsorption sites effectively. From Figure 8c we can note that for lower concentration values quantitative recovery of metal ions is compromised, though the elution efficiency increases with increasing HNO_3 concentration up to 2.0 mol L^{-1}, when practically 100% of the ions are desorbed. Greater HNO_3 concentrations provided nearly the same results as for the flow of 2.0 mol L^{-1}, but it is worth pointing out that exceedingly high HNO_3 concentrations may promote the oxidation of organic groups attached to the material's surface, thus reducing its adsorption capacity and usability. With the optimal preconcentration conditions, a study to uncover the material's maximum reuse cycles and chemical stability was performed, and the results are shown in Figure 8d. The material proved to maintain its maximum PF for 24 adsorption/desorption cycles when a decay in its efficiency was then noted. The material was also applied for the preconcentration of Cd(II) and Co(II), and the obtained results are summarized in Table 2. As can be noted, all metal ions presented a high PF (Cu = 18.1; Cd = 15.7; Co = 20.3), indicating that the material could be used for the preconcentration and determination of metal trace concentrations in aqueous samples. In addition, the same adsorption trend observed for the maximum adsorption capacity experiments in the batch regime could be seen reflected in the preconcentration experiments, which also points to a higher affinity of the material for the intermediary acids Co(II) and Cu(II), followed by the soft acid Cd(II) (compare the magnitude of the maximum adsorption capacities of the different metal ions in Table 1 with the respective magnitude of their preconcentration factors in Table 2).

Table 2. Preconcentration results obtained for Cu(II), Cd(II), and Co(II) using Si-AHTT as a solid sorbent in natural river water (Tietê River, São Paulo State, Brazil).

Metal species	Preconcentration factor	Metal concentration (μg L^{-1})*	After preconcentration (μg L^{-1})
Copper	18.1	9.94 ± 0.47	187.3 ± 9.45
Cadmium	15.7 ± 1.1	0.67 ± 0.008	12.80 ± 2.11*
Cobalt	20.3 ± 0.9	12.26 ± 0.52	239.54 ± 9.93
Standard reference material (SRM 1643e)			
	Certified values (μg L^{-1})	After preconcentration (μg L^{-1})	
Copper	22.20 ± 0.31	396.12 ± 8.34	
Cadmium	6.40 ± 0.07	105.81 ± 6.16	
Cobalt	26.40 ± 0.32	527.94 ± 9.47	

*Determination performed by GFAAS.

Table 2 also presents the results of the preconcentration system applied in trace metal determination for natural water from the Tietê River. The results obtained through direct determination using GFAAS present no difference from those obtained with the preconcentration system followed by FAAS determination. Furthermore, in order to confirm the good functioning and applicability of the proposed method, a standard water reference material (SRM 1643e) was subjected to the system. The results (Table 2) obtained are in agreement with the preconcentration factor experimentally determined and with the values provided by the manufacturer.

The cocondensation method could be effectively used to produce a silanized mesoporous SBA-15-type silica with a large surface area with globularly shaped particles. Characterization techniques along with a reutilization experiment also pointed to an efficient postfunctionalization of the material with 4-amino-5-hydrazino-1,2,4-triazole-3-thiol. The pseudo-second-order kinetic model was demonstrated to be an excellent model to describe the kinetic behavior of the material and indicated that chemisorption is the adsorption mechanism taking place. Despite its similar adsorption capacity in comparison to other adsorbents, Si-AHMT was demonstrated to be stable over a number of cycles of adsorption/desorption with a preconcentration factor of about 15-fold for all metal species, which could be useful for the determination of trace heavy metal ions in aqueous samples.

5. Experimental

5.1. Reactants and solutions

All reagents were of high purity or at least of analytical grade and used without previous purification. Solutions were prepared with deionized water collected from a Direct-Q system (Millipore, France). Metal ions solutions were prepared through the dissolution of its respective nitrate salts (Sigma-Aldrich, USA) followed by dilution to obtain the desired concentrations. Mesoporous modified silica was synthesized with the following reagents: surfactant triblock Pluronic P123 (P123), tetraethyl orthosilicate (TEOS; 99%), 3-choloropropyltriethoxysilane (CPTS; 95%), and the ligand molecule 4-amino-5-hydrazino-1,2,4-triazole-3-thiol (AHTT), which were purchased from Sigma-Aldrich (USA). Calibration solutions used in atomic absorption spectrometry determinations were prepared by appropriate dilution of stock standard solutions (1000 mg L^{-1}; Specsol, Brazil). Concentrated nitric acid (65%; Carlo Erba, France) used to prepare eluent solutions was predistilled in a quartz subboiling system (Marconi, Brazil) and the vessels used were washed with HNO_3 (10%, v/v) for at least 24 h, rinsed with deionized water, and dried at room temperature before use. The pH of solutions was adjusted by dripping either diluted HNO_3 or NaOH (99%; Impex, Brazil) solutions.

5.2. Equipment

In order to characterize the obtained material and its surface modification, the powders were subjected to infrared spectroscopy analysis using an FTIR spectrometer (Nicolet Nexus 670; Thermo, USA). Samples (KBr pellets of 200 mg containing 1% in mass of sample) were scanned 200 times at a resolution of 4 cm^{-1} in transmittance mode. Specific surface area measurements were carried out with a Micromeritics ASAP 2010 apparatus (USA), using 0.5 g of material. Elemental analysis was performed in a Thermo Finnigan Flash 1112 Series EA CHN elemental analyzer (USA) with 2.0 mg of material. Metal ion determination was performed with an atomic absorption spectrometer operating in flame mode (AAnalyst 700; PerkinElmer, USA), with 324.8, 240.7, and 228.8 nm as resonance lines for Cu(II), Co(II), and Cd(II), respectively. SEM images were collected with a Quanta 200 SEM (FEI Co., USA).

5.3. Preparation of modified mesoporous silica (Si-AHTT)

Mesoporous SBA-type silica was prepared through the cocondensation method, where 125 mL of 1.9 mol L^{-1} HCl (37%, Carlo Erba) solution and 4.0 g of P123 were added into a 250-mL beaker. It was kept under stirring and heating (40 °C) until the complete dissolution of the surfactant. Then 5.0 mL of TEOS was added to the initial solution and, after 30 min, 2.0 mL of CPTS was also added. The mixture was kept under heating and

stirring for 20 h. The obtained product was aged in a drying oven at 100 °C for 24 h and then it was separated from the supernatant through vacuum filtration. The product, named Si-CPTS, was washed in order to remove the surfactant with ethanol/water (50% v:v) in a Soxhlet system for 72 h, dried, and properly stored. For the substitution of the Cl atoms of the CPTS by the ligand molecule, 25 mL of DMF (99.8 %, Sigma-Aldrich) and 1.0 g of AHTT were added to a reaction flask. The mixture was stirred at 140 °C until complete dissolution. Then the Si-CPTS was added to the reaction flask and the mixture was further stirred under heating for 24 h. Afterwards, the product named Si-AHTT was washed in a beaker with hot DMF and in a Soxhlet system with ethanol/water (50% v:v) for 48 h. The reaction and application scheme for the synthesized material is depicted in Figure 9.

5.4. Determination of point of zero charge (PZC)

In order to obtain more information about the surface charge of the material, an experiment to determine its PZC was performed. In this experiment 20.0 mg of Si-AHTT was added to 12 flasks containing 20 mL of KNO_3 (Sigma-Aldrich) as 0.1 mol L^{-1} solutions, whose pH was adjusted to values from 1 to 12. The solutions had their pH adjusted through the addition of either HCl or NaOH solutions. The mixtures were stirred for 24 h prior the measurement of the final pH.

5.5. Batch adsorption experiments

All batch adsorption experiments were performed using 50.0 mg of the material and 20.0 mL of metal solution. The mixtures were stirred and filtered under vacuum and the supernatant had its concentration determined through FAAS with a Shimadzu AA7000 spectrometer (USA). Kinetic experiments were conducted within a time interval from 1 to 180 min while the metal concentration and pH of the solutions were set to 40 mg L^{-1} and $\sim$6. In an experiment to determine the maximum adsorption capacity of the material, dynamic contact time was fixed at 50 min, solution pH was $\sim$6, and metal solution concentration was varied from 5 to 130 mg L^{-1}.

5.6. Column and preconcentration experiments

Metal adsorption in column mode was investigated using 20 mg of Si-AHTT packed in a Tygon tube with 2.86 mm internal diameter and the flow was induced by a peristaltic pump (DMC 100, Tecnopon, Brazil). The material was stopped inside the column by using glass wool at both sides of the packed material, and the preconcentration system was optimized by percolating 20.0-mL aliquots of 20 μg L^{-1} Cu(II) solution (pH ca. 5–6). Sample and eluent (HNO_3 solutions) flows were investigated from 0.5 to 5.0 mL min^{-1}, and eluent concentration was investigated in a range from 0.5 to 4.0 mol L^{-1} of a solution of nitric acid. Column reuse was investigated for up to 30 adsorption desorption cycles. Eluate was collected in polyethylene flasks, followed by metal determination by FAAS. The preconcentration factor was calculated by Eq. (4):

$$PF = \frac{C_e}{C_p}, \tag{4}$$

where C_e is the eluent concentration determined after the preconcentration procedure and C_p is the concentration of percolated solution (20 μg L^{-1}).

5.7. Sample preparation and metal determination in natural water samples

Surface water samples were collected from the Tietê River (Borborema, São Paulo State, Brazil) using a polyethylene bottle, without acidification, and immediately filtered through a 0.45-μm membrane. Filtered samples were subjected to a digestion procedure according to a previously published work.[44] Metal determination in mineralized water was performed directly by GFAAS and by FAAS after the preconcentration step. In order to validate the results obtained with the developed method, a standard water reference material (SRM 1643e) was subjected to the preconcentration system and the results were compared with those provided by the National Institute of Standards and Technology.

Acknowledgments

The authors thank Fundacão de Amparo à Pesquisa do Estado de São Paulo (FAPESP; Proc: 2012/21795-9, 2015/04791-8, 2015/05224-0, and 2013/22955-2) and CNPq (Proc: 302284/2012-5). The authors also thank the Centro de Microscopia Eletrônica (CME) of the Institute of Biosciences of UNESP (Botucatu).

References

1. Tóth, G.; Hermann, T.; Silva, M. R.; Montanarella, L. *Environ Int.* **2016**, *88*, 299-309.
2. David, I. G.; Matache, M. L.; Tudorache, A.; Chisamera, G.; Rozylowicz, L.; Radu, G. L. *Eng. Manag. J.* **2012**, *11*, 69-73.
3. Minello, M. C. S.; Paçó, A. L.; Martines, M. A. U.; Caetano, L.; Santos, A.; Padilha, P. M.; Castro, G. R. *J. Environ. Sci. Health. A* **2009**, *44*, 861-865.
4. Chien, L. C.; Hung, T. C.; Choang, K. Y.; Yeh, C. Y.; Meng, P. J.; Shieh, M. J.; Han, B. C. *Sci. Total Environ.* **2002**, *285*, 177-185.
5. Manahan, S. E. *Environmental Science and Technology*. CRC Press: Boca Raton, FL, USA, 2000.
6. Mirzaei, M.; Behzadi, M.; Abadi, N. M.; Beizaei, A. *J. Hazard. Mater.* **2011**, *186*, 1739-1743.
7. Mohammadia, S. Z.; Afzali, D.; Baghelan, Y. M. *Anal. Chim. Acta* **2009**, *653*, 173-177.
8. Ghaedi, M.; Shokrollahi, A.; Niknam, K.; Niknam, E.; Soylak, M. *Cent. Eur. J. Chem.* **2009**, *7*, 148-154.
9. Jorgetto, A. O.; Silva, R. I. V.; Longo, M. M.; Saeki, M. J.; Padilha, P. M.; Martines, M. A. U.; Rocha, B. P.; Castro, G. R. *Appl. Surf. Sci.* **2013**, *264*, 368-374.
10. Martins, A. E.; Pereira, M. S.; Jorgetto, A. O.; Martines, M. A. U.; Silva, R. I. V.; Saeki, M. J.; Castro, G. R. *Appl. Surf. Sci.* **2013**, *276*, 24-30.
11. Gurgel, L. V. A.; Freitas, R. P.; Gil, L. F. *Carbohyd. Polym.* **2008**, *74*, 922-929.
12. Kalmykova, Y.; Strömvall, A. M.; Steenari, B. M. *J. Hazard. Mater.* **2008**, *152*, 885-891.
13. Feist, B.; Mikula, M. *Food Chem.* **2014**, *147*, 225-229.
14. Bulut, V. N.; Duran, C.; Gundogdu, A.; Soylak, M.; Yildirim, N.; Elci, L. *Talanta* **2008**, *76*, 469-474.
15. Bulut, V. N.; Arslan, D.; Ozdes, D.; Soylak, M.; Tefekci, M. *J. Hazard. Mater.* **2010**, *182*, 331-336.
16. Jorgetto, A. O.; Silva, R. I. V.; Saeki, M. J.; Barbosa, R. C.; Martines, M. A. U.; Jorge, S. M. A.; Silva, A. C. P.; Schneider, J. F.; Castro, G. R. *Appl. Surf. Sci.* **2014**, *288*, 356-362.
17. Hossain, M. A.; Ngo, H. H.; Guo, W. S.; Setiadi, T. *Bioresource Technol.* **2012**, *121*, 386-395.
18. Ali, R. M.; Hamad, H. A.; Hussein, M. M.; Malash, G. F. *Ecol. Eng.* **2016**, *91*, 317-332.
19. Yadav, S. K.; Singh, D. K.; Sinha, S. *J. Environ. Chem. Eng.* **2014**, *2*, 9-19.

20. Wondracek, M. H. P.; Jorgetto, A. O.; Silva, A. C. P.; Ivassechen, J. R.; Schneider, J. F.; Saeki, M. J.; Pedrosa, V. A.; Yoshito, W. K.; Colauto, F.; Ortiz, W. A. et al. *Appl. Surf. Sci.* **2016**, *367*, 533-541.
21. Filho, E. S. S.; Melo, J. C. P.; Fonseca, M. G.; Airoldi, C. *J. Colloid Interf. Sci.* **2009**, *340*, 8-15.
22. Melo, J. C. P.; Filho, E. C. S.; Santana, S. A. A.; Airoldi, C. *J. Colloid Interf. Sci.* **2009**, *346*, 138-145.
23. Pizarro, J.; Castilho, X.; Jara, S.; Ortiz, C.; Navarro, P.; Cid, H.; Rioseco, H.; Barros, D.; Belzile, N. *Fuel* **2015**, *156*, 96-102.
24. Prado, A. G. S.; Airoldi, C. *Anal. Chim. Acta* **2001**, *432*, 201-211.
25. Ferreira, G.; Caetano, L.; Castro, R. S. D.; Padilha, P. M.; Castro, G. R. *Clean Technol. Envir.* **2011**, *13*, 397-402.
26. Ezzeddine, Z.; Batonneau-Gener, I.; Pouilloux, Y.; Hamad, H.; Saad, Z.; Kazpard, V. *Micropor. Mesopor. Mat.* **2015**, *212*, 125-136.
27. Anbia, M.; Kargosha, K.; Khoshbooei, S. *Chem. Eng. Res. Des.* **2015**, *93*, 779-788.
28. Ali, L. I. A.; Ibrahim, W. A. W.; Sulaiman, A.; Kamboh, M. A.; Sanagi, M. M. *Talanta* **2016**, *148*, 192-199.
29. Aboufazeli, F.; Zhad, H. R. L. Z.; Sadeghi, K. M.; Najafi, E. *Food Chem.* **2013**, *141*, 3459-3465.
30. Wang, Z.; Xu, J.; Hu, Y.; Zhao, H.; Zhou, J.; Liu, Y.; Lou, Z.; Xu, X. *J. Taiwan Inst. Chem. Eng.* **2016**, *60*, 394-402.
31. El-Toni, A. M.; Habila, M. A.; Ibrahim, M. A.; Labis, J. P.; Alothman, Z. A. *Chem. Eng. J.* **2014**, *251*, 441-451.
32. Hao, S.; Zhong, Y.; Pepe, F.; Zhu, W. *Chem. Eng. J.* **2012**, *189*, 160-167.
33. Souza, E. J.; Cristante, V. M.; Padilha, P. M.; Jorge, S. M. A.; Martines, M. A. U.; Silva, R. I. V.; Carmo, D. R.; Castro, G. R. *Pol. J. Chem. Technol.* **2011**, *13*, 28-33.
34. Ferreira, G.; Caetano, L.; Castro, R. S. D.; Padilha, P. M.; Castro, G. R. *Clean Techn. Environ. Policy.* **2011**, *13*, 397-402.
35. Tobiasz, A.; Walas, S.; Landowska, L.; Góral-Konefal, J. *Talanta* **2012**, *96*, 82-88.
36. Mashkani, M.; Mehdinia, A.; Jabbari, A.; Bide, Y.; Nabid, M. R. *Food. Chem.* **2018**, *239*, 1019-1026.
37. Sing, K. S. W.; Everett, D. H.; Haul, R. A. W.; Moscou, L.; Pierotti, R. A.; Rouquerol, J.; Siemieniewska, T. *Pure Appl. Chem.* **1985**, *57*, 603-619.
38. Brunauer, S.; Demning, L. S.; Demning, W. S.; Teller, E. *J. Am. Chem. Soc.* **1940**, *62*, 1723-1732.
39. Mason, G. *J. Colloid Interf. Sci.* **1982**, *88*, 36-46.
40. McBain, J. W. *J. Am. Chem. Soc.* **1935**, *57*, 699-700.
41. Urus, S.; Purtas, S.; Ceyhan, G.; Tümer, F. *Chem. Eng. J.* **2013**, *220*, 420-430.
42. Jorgetto, A. O.; Silva, A. C. P.; Wondracek, M. H. P.; Silva, R. I. V.; Velini, E. D.; Saeki, M. J.; Pedrosa, V. A.; Castro, G. R. *Appl. Surf. Sci.* **2015**, *345*, 81-89.
43. Pearson, G. R. *J. Am. Chem. Soc.* **1963**, *85*, 3533-3539.
44. Castro, G. R.; Caetano, L.; Ferreira, G.; Padilha, P. M.; Saeki, M. J.; Zara, L. F.; Martines, M. A. U.; Castro, G. R. *Ind. Eng. Chem. Res.* **2011**, *50*, 3446-3451.